www.lajss.org
Latin American Journal of Solids and Structures 5 (2008)289–317

The energy absorption characteristics of double-cell tubular profiles

S. Chung Kim Yuen*, G.N. Nurick and R.A. Starke

Blast Impact and Survivability Research Unit (BISRU), Department of Mechanical Engineering, University of Cape Town, Private Bag, Rondebosch 7701, South Africa.

Abstract

This article presents the results of experimental work on the crushing characteristics of single-cell and double-cell mild steel profiles with different dimensions and cross-sectional shape. The energy absorption characteristics and mode of collapse of seven double-cell profiles containing square and/or circular tubes is investigated with a view to finding the cell combination with the highest energy absorption characteristics. Double-cell profiles made with circular tubes have higher energy absorption efficiencies than those made with square tubes. Equivalent single-cell circular tube can be more efficient than the double-cell tube depending on the loading conditions. For all the configurations, the mode of collapse of the double-cell profile is initially dominated by the outer tube. In some configurations after the initial collapse, the inner tube crushing mode becomes more dominant; resulting in Euler collapse mode.

Keywords: Tubes, Crushing, Crashworthiness, Energy absorption, Tubes in parallel.

Notations

σ_y	static yield stress
δ	Crush distance
ϕ	Solidity ratio
η	material constant
A	Cross sectional area
A_c	Enclosed cross-sectional area
C	Tube width
CFE	Crush force efficiency
CM	Crush mode
D	strain rate material constant
E_{pd}	Potential energy
H	Tube thickness
M	Drop mass
M_o	Plastic moment
P_m	Mean crush force

*Corresp. author. Email: steeve.chungkimyuen@uct.ac.za Received 17 Jun 2008; In revised form 12 Sep 2008

P_m^d	Mean crush force from dynamic test
P_m^s	Mean crush force from quasi static test
P_{ult}	Ultimate peak force
P_{ult}^s	Ultimate peak force from quasi-static test
R	Tube radius
V_i	Impact velocity

1 Introduction

With the potential for accidents due to the ever-increasing demand for mass transport and many other practical engineering systems, the requirements for absorbing energy during impact events have become a necessity. Numerous energy absorbers have been developed to dissipate energy in different ways using different materials and structures. An ideal energy absorber, in many of these applications, should be as light as possible in weight but strong enough to maintain the maximum constant and controlled allowable retarding force throughout the greatest possible displacement (stroke length). With respect to these demands, the large plastic deformation of thin-walled metal tubes that buckle progressively is a very simple and highly effective way of absorbing energy during impact events [14, 24]. Such thin-walled structures, inexpensive and versatile, are used in numerous engineering applications including collision protection for transport systems [1, 2, 27].

Studies on the axial crushing behaviour of thin-walled structures, ongoing for the past five decades, have been overviewed by Reid [29], Alghamdi [3], Jones [15] and Chung Kim Yuen and Nurick [45]. Reid [29] focussed on the progressive buckling, inversion and splitting of circular tubes. Alghamdi [3] briefly reviewed the common shapes of collapsible energy absorbers such as circular tubes, square tubes, frusta, struts, honeycombs and sandwich plates and their most common deformation shapes. Jones [15] discussed the dynamic plastic instability of different circular and square tubes subjected to large axial impact loads. Chung Kim Yuen and Nurick [45] presented an overview on studies investigating the effect of different types of triggers on the crushing characteristics of tubular structures. One of the common goals of most of these studies is to improve the energy absorption characteristics of the tubular structures by any means, for instance triggers [4, 6, 7, 20, 23, 25, 26, 34, 38, 42–44] or stiffeners [5, 16–18, 36, 40, 41].

Various authors have also tried to increase the energy absorption of thin-walled tubes with the use of fillers [10–13, 19, 21, 22, 28, 30, 31, 35, 37, 39]. The addition of fillers, cellular material such as honeycombs, wood and foam, to the tubular structure is a common method which dramatically improves the energy absorption efficiency of the tube. The filler itself absorbs energy by plastic deformation and, depending on its density, may change the tube's original mode of collapse into a more efficient mode of collapse.

Seitzberger et al. [32,33] increased the energy absorption capabilities of thin-walled tubes by

using a double cell profile (two tubes with similar cross-section one placed concentrically inside the other) arrangements, empty or filled with aluminium foam. The results for the experiments, carried out quasi-statically, confirmed that considerable mass efficiency improvements with respect to energy absorption could be obtained despite a reduction in stroke lengths caused by the presence of foam. Figure 1 shows progressive buckling, i.e. the sequential formation of adjacent local folding patterns of the different specimens. Distinct differences were pointed out between the different cross-sectional shapes. Hexagonal and octagonal members were more efficient than square cross-sections. The double cell arrangements were shown to be particularly efficient crush elements, as long as global failure (Euler buckling) could be avoided. The study also showed that double cell arrangements may be preferable to single tube based on mass specific energy absorption because the inner tube is more mass efficient.

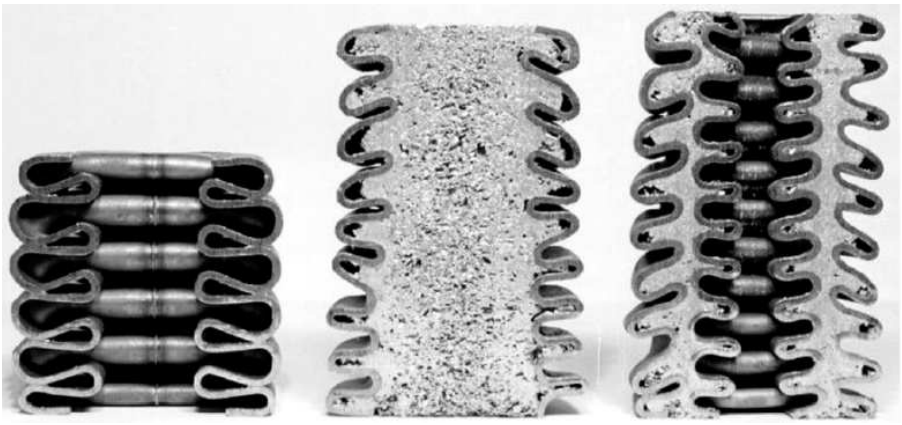

Figure 1: Empty, Monotubal filled and Bitubal Square crushed specimens[43].

Zhao et al. [8, 46, 47] also carried out quasi-static tests on different double cell arrangements, filled with concrete, as energy absorbing members in buildings located in earthquake zones, service conduits carrying utilities through buildings and undersea applications. The double cell arrangements (double-skin tubes) were of different configurations, namely square tubes as both inner and outer, circular tubes as both inner and outer and circular tube as outer tube with an inner square tube. It was found that there was an increase in ductility for concrete filled double-skin tubes in compression when compared to empty single skin tubes. The main conclusions drawn from these studies that concrete filling enhances strength, ductility and energy absorption of the hollow tube, particularly for higher diameter-to-thickness ratio (D_t/H) ratios. This was due to confinement of the core concrete and restraining the steel tube jacket against local buckling. The mode of collapse of the outer tube was independent of the inner tube but the mode of collapse of the inner was dependent on the surrounding concrete.

This paper reports on the results of an investigation into the response of double cell arrangements with no fillers to quasi-static and dynamic axial load. Different configurations, square

tubes as both inner and outer, circular tubes as both inner and outer, circular tube as outer tube with an inner square tube and square tube as outer tube with an inner circular tube, are investigated with a view to characterise the collapse mode and energy absorption characteristics.

2 Experiments

2.1 Quasi-static axial compression

The quasi-static tests are performed, on a 200kN rated Zwick testing machine that records the axial load-displacement histories at a constant pre-set cross-head speed. Using theoretical calculations from Jones [14], the maximum peak force could be predicted for various locally available standard tubes sizes. The largest tube sizes are selected so that their theoretical maximum force is within the equipment's rated load. The smaller tubes are selected so that a varying degree of interaction would occur during the crushing. Three sizes of circular and square tubes, listed in Table 1, are used as 'base' tubes. The nominal thickness of the tubes is 1.6mm. All tubes are 140 mm long with a crushable length of 90mm or 130 mm. The rest of the tube is clamped in a locking mechanism. From the six 'base' tubes seven double wall combination tubes are assembled. These combinations are based on two types of outer tubes, ϕ 50.8 mm circular and 50.8mm square. Schematics of the different assembled double wall tubes are shown in Figure 2.

Table 1: Nominal properties of tubes

Tube (mm)	**Types**	**Notation**	**Mass (g)**	σ_y **(MPa)**
ϕ25.4	Circular	C25	130	291
ϕ38.1	Circular	C38	193	352
ϕ50.8	Circular	C50	265	304
25.4 x 25.4	Square	S25	160	310
38.1 x 38.1	Square	S38	24	287
50.8 x 50.8	Square	S50	320	275

The inner tube is located with respect to the outer tube throughout the duration of the experiment by means of a tube locator, shown in Figure 3(a). Due to the geometry of the tube combinations 7 different tube locators are machined from mild steel block, all are 10 mm thick. The assembled clamped specimen, shown in Figure 3(b), is placed onto the moving bed of the test machine in such a way that the specimen is carefully positioned at the centre of the cross-head with the end faces exactly perpendicular to the longitudinal axes for the quasi-static tests. The specimen is then sandwiched against a flat stationary steel plug which is parallel to the bottom clamping device to ensure a uniform distributed load.

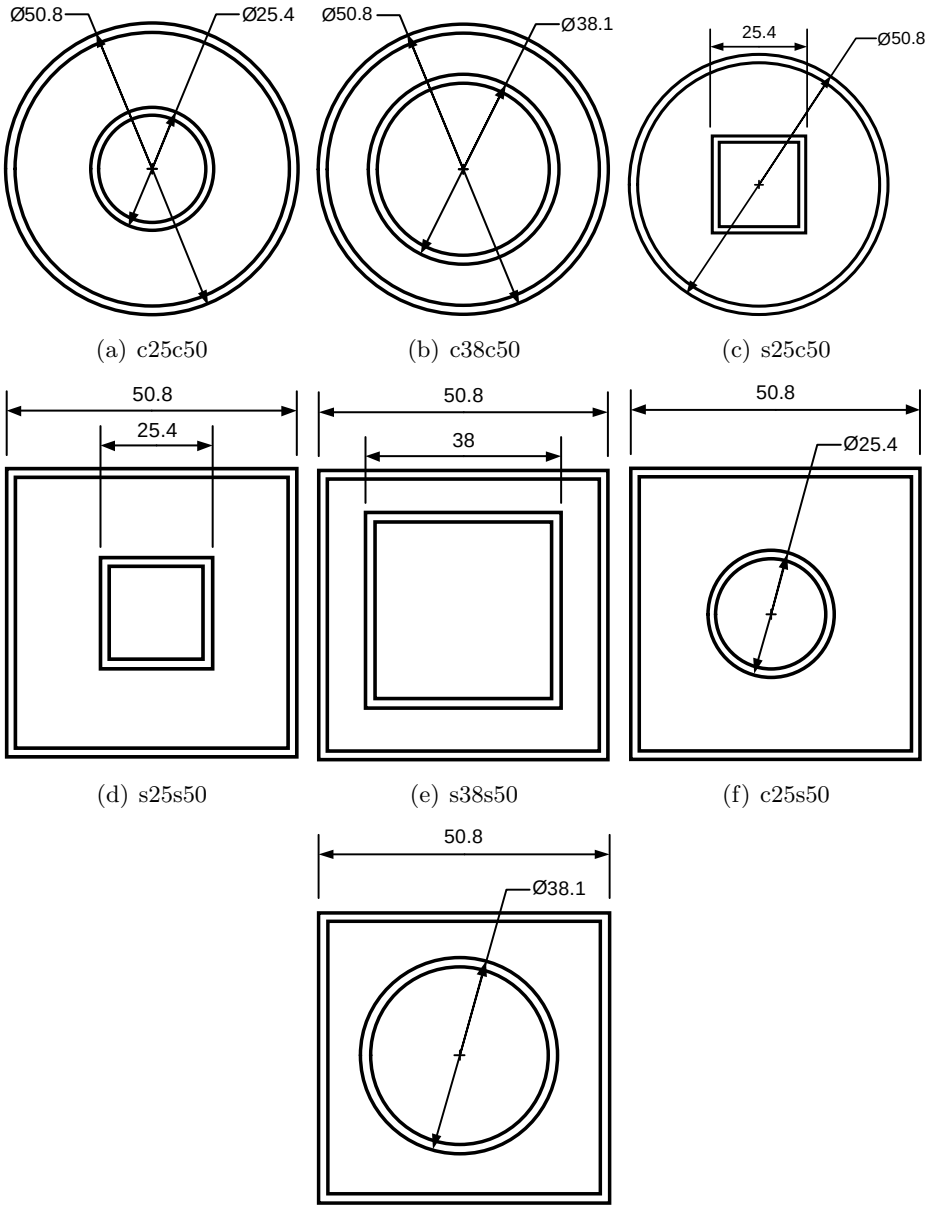

(a) c25c50 (b) c38c50 (c) s25c50

(d) s25s50 (e) s38s50 (f) c25s50

(g) c38s50

Figure 2: Schematic of specimen sizes and configurations used

(a) (b)

Figure 3: Example of (a) a tube locator and (b) specimen in the clamp (c38s50)

2.2 Single-cell tubes subjected to quasi-static loading

Table 2 lists a summary of the single cell tube's crush behaviour. The cross head displacement and the final crush deflection are not the same as the tube experiences a small elastic recovery once the load is removed. However, this deformation is negligible compared to the plastic deformation and, hence, is neglected. For this reason the cross head displacement is taken to be the same as the crush displacement.

Figure 4 shows the transient response of a 38mm square tube to a quasi-static axial load. The first lobe is formed at the bottom end of the tube (where the bed moves). Subsequent folds are developed and progress to the non-moving end of the tube. Figure 5 shows the axial force-displacement curve obtained from the crush of two separate tests of the same tube configuration. Sub-labels (a) - (j) shown in Figure 4 correspond to the different stages of the lobes development sub-labelled (a) - (j) in Figure 5. An ultimate peak load of 80kN is reached prior the formation of the first lobe. Thereafter, a repeated pattern of load-displacement behaviour of different load magnitude which is associated with the sequential development of lobe is exhibited. The mean crush load is 30kN.

Table 2: Quasi-static crushing results for single cell tubes

Specimen	**Free Length (mm)**	δ**(mm)**	P_m^s **(kN)**	P_{ult}^s **(kN)**	**CM**
c25q1	130	30.43	13.02	43.67	Euler
c25q2	90	64.92	30.37	46.04	Mixed
c25q3	130	28.02	13.28	41.31	Euler
c25q4	130	21.42	18.58	41.28	Euler
c25q5	90	68.83	29.60	42.32	Mixed
c25q6	90	67.92	29.07	43.40	Mixed
c38q2	130	90.79	45.91	81.21	Mixed
c38q3	130	90.76	38.16	72.00	Mixed
c38q4	130	90.49	43.44	76.60	Asymmetric
c50q1	130	69.27	43.78	85.47	Asymmetric
c50q2	130	90.50	42.52	83.57	Asymmetric
s25q1	130	84.87	32.34	62.11	Symmetric
s25q2	130	34.61	22.81	62.87	Euler
s25q3	90	50.65	31.97	62.66	Symmetric
s25q4	130	27.28	24.80	62.90	Euler
s25q6	130	32.37	22.28	55.47	Euler
s25q7	90	63.88	33.02	61.82	Symmetric
s25q8	90	63.57	32.83	62.02	Symmetric
s38q1	130	91.94	23.05	72.26	Symmetric
s38q2	130	91.04	30.29	80.51	Symmetric
s50q1	130	89.89	30.47	90.82	Symmetric
s50q2	130	97.25	22.23	83.50	Symmetric

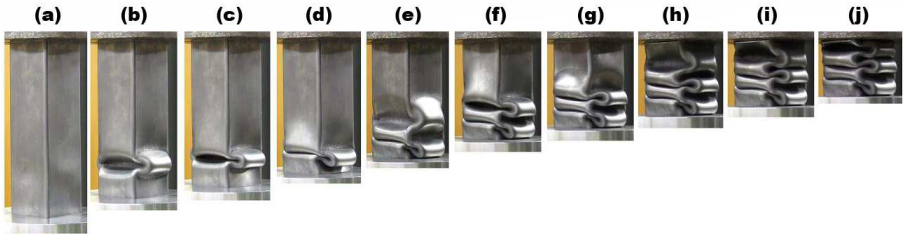

Figure 4: Progressive collapse of a 38.1 x 38.1mm square tube.

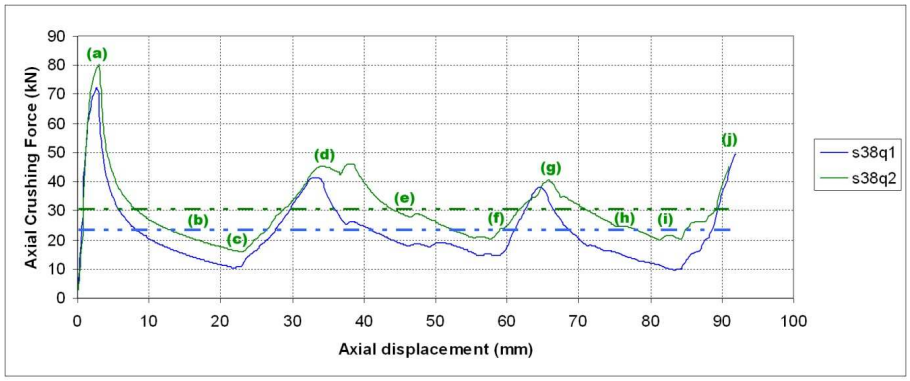

Figure 5: Force-displacement curve for 38.1 x 38.1mm square tubes.

2.3 Double cell tubes subjected to quasi-static loading

Table 3 lists a summary of the crush behaviour of double cell tube. The overall crush mode of the double cell tube is progressive and is influence by the crush mode of the inner tube which appears to dictate the crush behaviour of the double cell. The ultimate peak and mean crush force of the double cell tubes is characterised by the addition of the ultimate peak and mean forces of the single cell tubes respectively, (see Figures 12-18). For instance, for a c25c50, the ultimate peak force is about 125kN which equivalent to the sum of the ultimate peak force of a c25 tube, 43kN, and a c50 tube, 82kN.

Table 3: Quasi-static crushing results for double cell tubes

Specimen	δ**(mm)**	P_m^s **(kN)**	P_{ult}^s **(kN)**	**Inner CM**	**Outer CM**
c25c50q1	70.48	67.10	127.77	Euler	Mixed
c25c50q2	25.36	73.54	125.82	Euler	Asymmetric
c38c50q1	90.79	93.46	157.85	Mixed	Mixed
c38c50q2	90.76	95.14	162.08	Mixed	Mixed
c38c50q3	90.75	95.25	165.09	Mixed	Mixed
s25c50q1	89.03	73.93	144.32	Euler	Mixed
s25c50q1	45.57	78.31	145.26	Euler	Mixed
s25s50q1	89.03	68.60	154.08	Symmetric	Symmetric
s25s50q2	63.73	63.79	152.93	Euler	Symmetric
s38s50q1	90.78	68.78	178.94	Symmetric	Symmetric
s38s50q2	87.86	69.94	179.59	Symmetric	Symmetric
c25s50q1	43.93	55.80	134.66	Euler	Symmetric
c38s50q1	84.87	78.96	170.11	Asymmetric	Symmetric
c38s50q2	74.24	74.72	167.66	Asymmetric	Symmetric

Figure 6 shows specimens with 50mm circular and square outer tubes and 25mm circular and square inner tubes. In all but one case, the inner 25mm tube buckles in Euler Mode; highlighted in Figure 6(a). Progressive buckling is initiated in the outer tube until the inner tube interacts with the outer tube changing its mode of failure, destabilising the overall buckling mode. In the one exception, Figure 6(d), both the inner and outer square tubes buckle progressively with minimal interaction and interference with one another. The smaller inner tube has more lobes formed.

Figure 7 shows the axial crushing force displacement of the c38c50 double cell tubes. The cyclic loading is typical of that of a single cell tube. In all three c38c50 specimens, both inner and outer tubes initially deformed in concertina mode (The plastic hinges form around the circumference of the tube at the top axi-symmetrically. The tube deforms to form sequential folding in ring shaped lobes along the length of the tube [14]) and switched to diamond mode (The tube buckles progressively by forming sequential folds accompanying a change in the cross-section shape of the tube. Diamond shaped sections around the circumference of the tube with different number of lobes are obtained [14]). During the axisymmetric collapse there is minor interaction between the tubes at the top end, highlighted in Figure 8. Once buckling mode switches to diamond mode more interactions between the tubes is observed at the non impact end.

Figure 9(a) and (b) shows the side and section view of double cell tubes with 50mm outer square tubes and 38mm circular and square inner tubes respectively. In both cases, the inner tubes buckle in such a way that the lobe formation matches that of outer tubes. The sequential development of lobes for a c38s50 double cell tube subjected to quasi-static axial load is shown in Figure 10 with its corresponding axial force-displacement curve shown in Figure 11. Sub-labels (a) - (g) shown in Figure 10 correspond to the different stages of the lobes development sub-labelled (a) - (g) in Figure 11. An ultimate peak load of 170kN is reached prior to the formation of the first lobe. Thereafter, a repeated pattern of load-displacement behaviour which is associated with the sequential development of lobe is exhibited, as observed for single cell tubular structure. The mean crush load is 79kN.

Figures 12-18 show the axial force displacement curves of the quasi-static test for a single inner cell, a single outer cell and a double cell profile consisting of both an inner and outer tube. The 25mm circular tube buckles in Euler mode in all cases. Consequently the axial force is considered constant once the test is stopped (Figure 12 and Figure 17). In cases where all three cells buckle progressively, the wavelengths indicate the lobe size of the different cells. The wavelength of the double cell profile matches that of the outer tube suggesting that the larger outer tube determines the wrinkle wavelength in the double-cell profile. However, after a certain axial displacement, depending on the inner tube, the double cell profile appears to follow the force-displacement characteristics of the inner tube and not the outer tube. This suggests that inner tube dictates the crushing characteristics of the multi-cell profile past that crushing distance. The addition of the axial forces of the inner and outer tubes is also plotted and compared to the double cell profile. The two curves display similar characteristics with

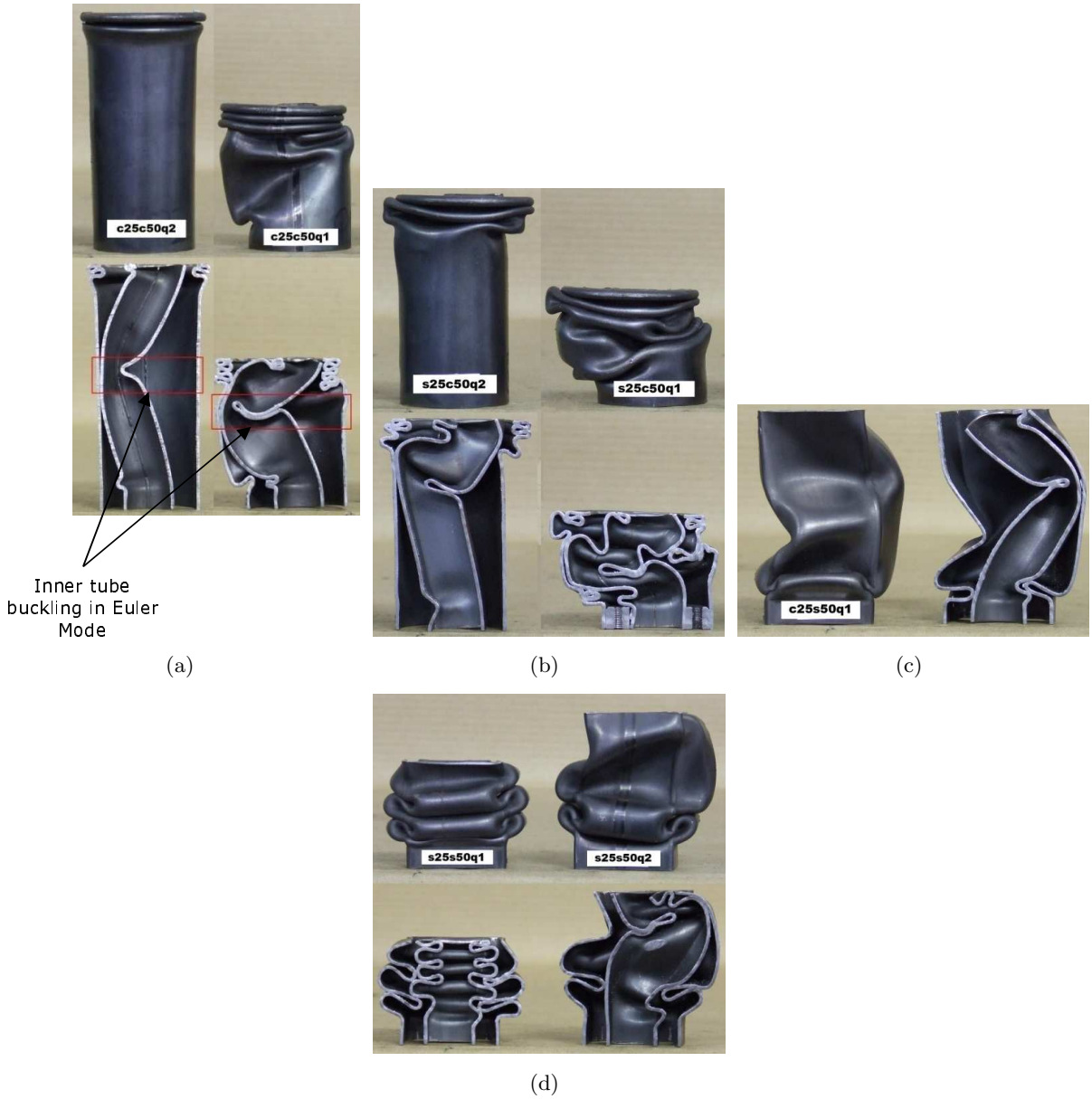

(a) (b) (c)

(d)

Figure 6: Side and section view of quasi-statically crushed (a) c25c50 (b) s25c50 (c) c25s50 (d) s25s50.

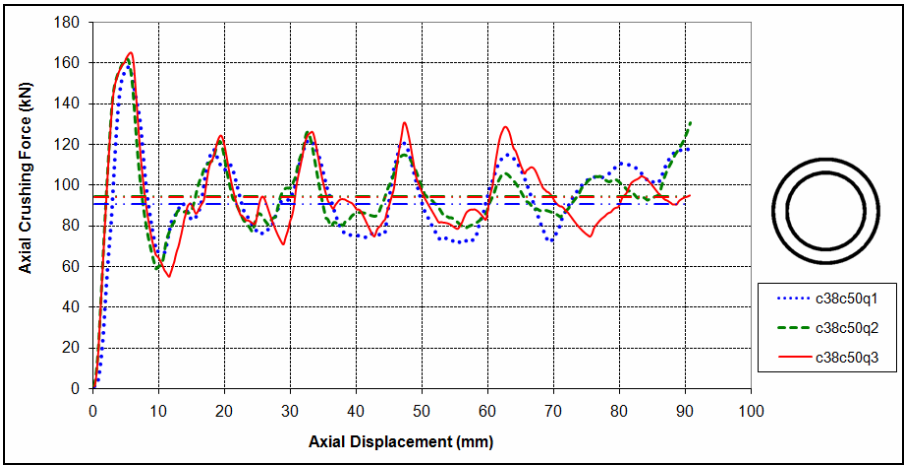

Figure 7: Force-displacement curve for c38c50.

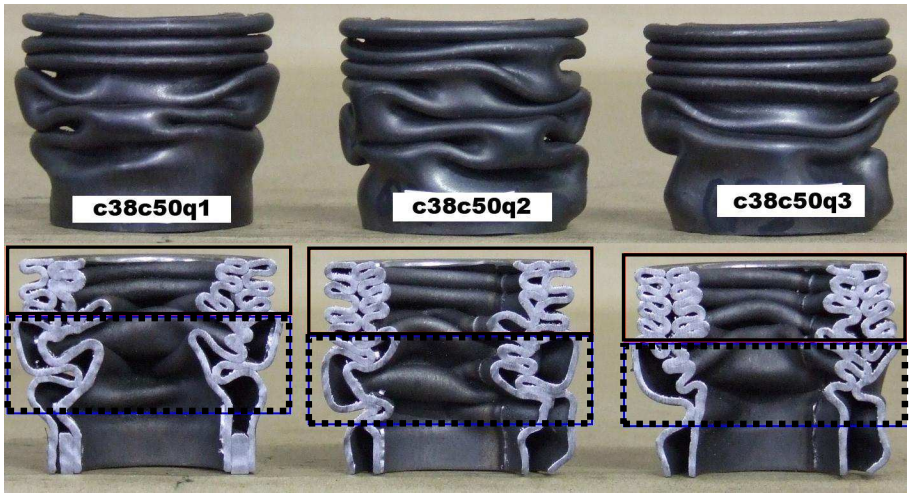

Figure 8: Side and section view of quasi-statically crushed c38c50.

(a) (b)

Figure 9: Side and section view of quasi-statically crushed (a) c38s50 (b) s38s50.

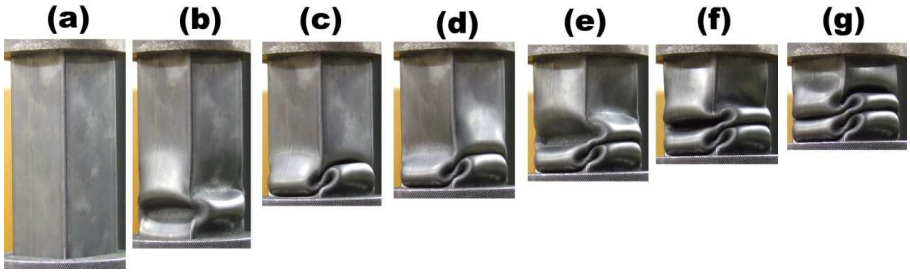

Figure 10: Progressive collapse of c38s50q1.

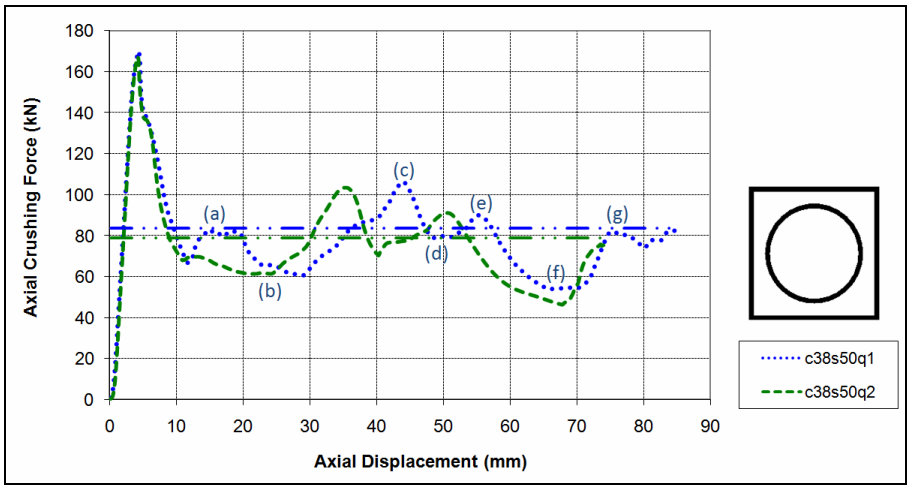

Figure 11: Force-displacement curve for c38s50.

the double cell profile curves exhibiting slightly higher forces compared to the added forces of the inner and outer profile. This may be due to interaction between the two tubes which may provide extra resistive crushing force and is not considered in the added profile.

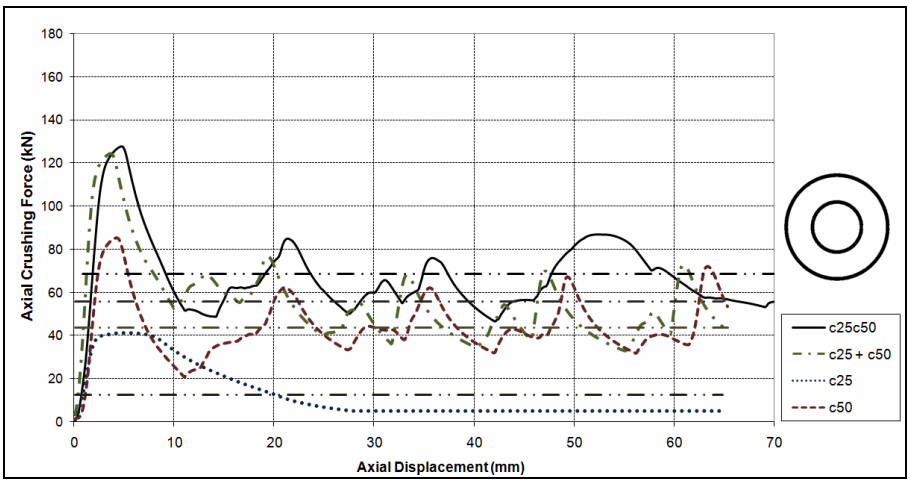

Figure 12: Force-displacement curve for c25c50 profile

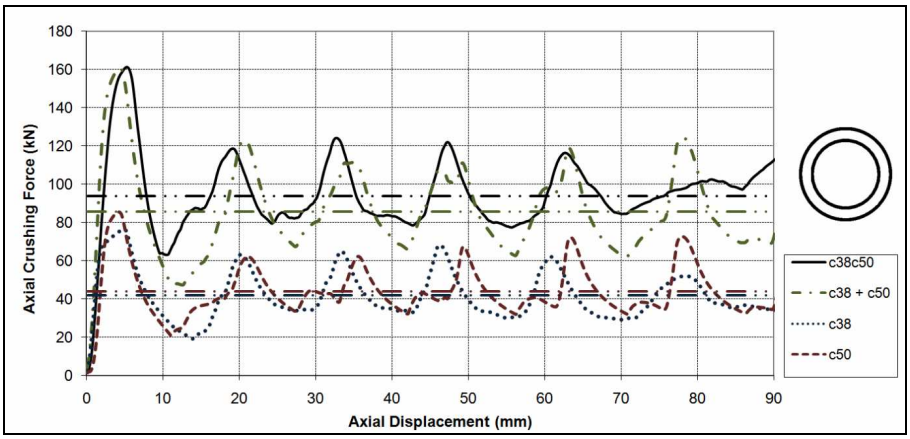

Figure 13: Force-displacement curve for c38c50 profile

The quasi-static results are analysed by comparing their specific energies which is defined as the ratio of the energy absorbed through plastic deformation to the total mass of the absorber [14]. As a result of the different yield stress of the different tubular profile, the results are normalised. For double-cell profiles, the yield stress is averaged between the two yield stresses of the separate tubes. The cross-sectional area of the double-cell profile is also converted to an equivalent single cell tube, illustrated in Figure 19, having the dimensions of the outer tubes

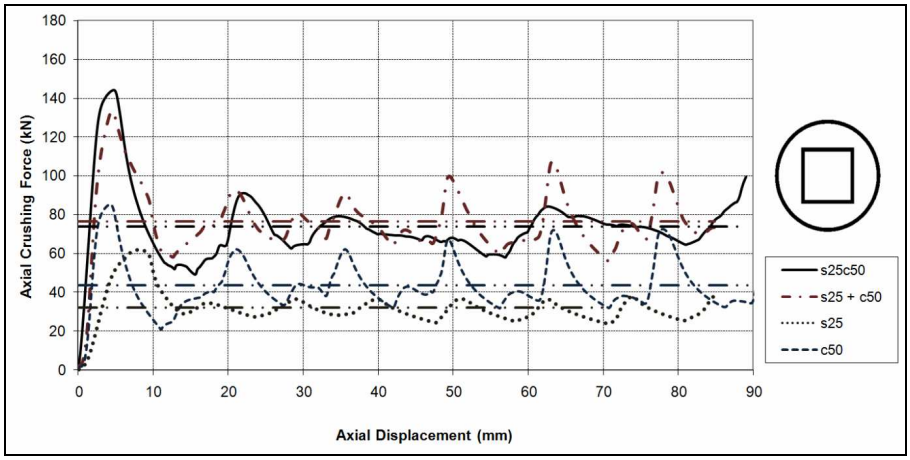

Figure 14: Force-displacement curve for s25c50 profile

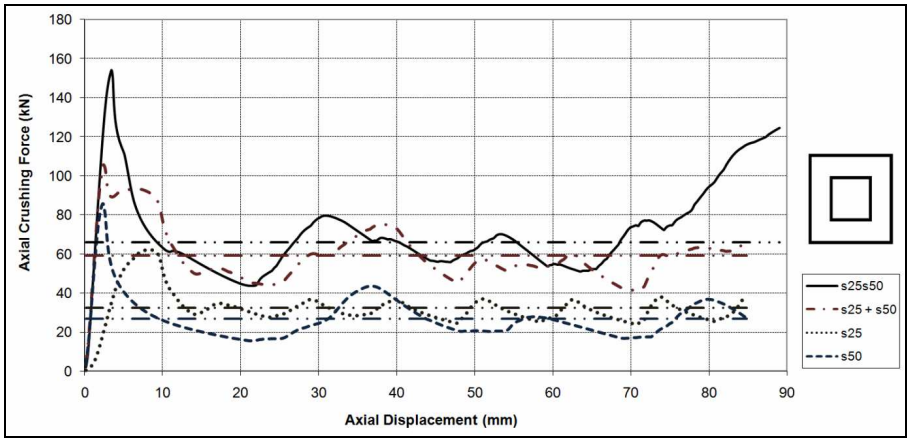

Figure 15: Force-displacement curve for s25s50 profile

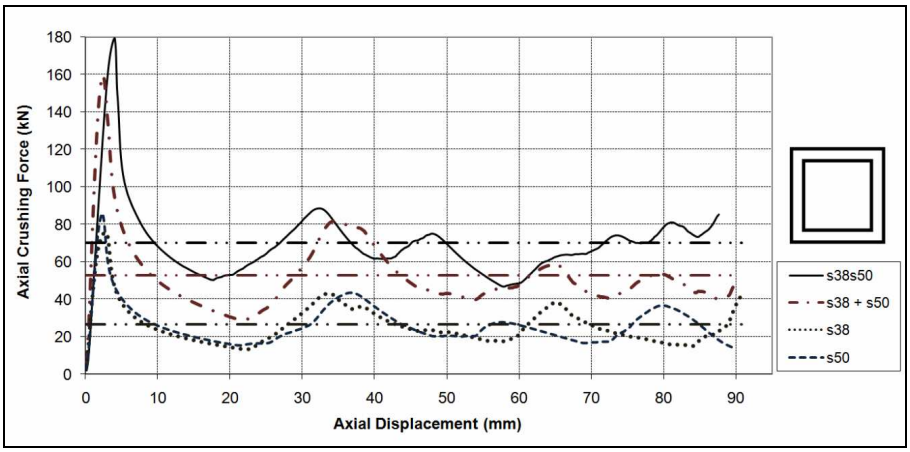

Figure 16: Force-displacement curve for s38s50 profile

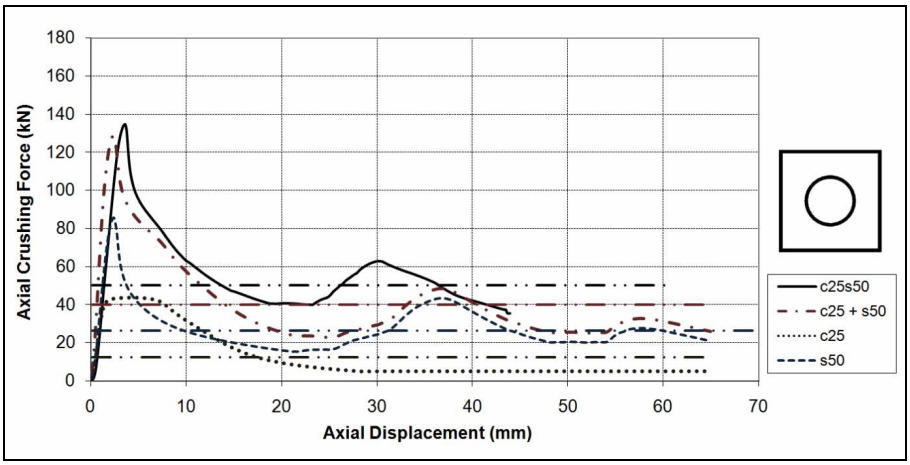

Figure 17: Force-displacement curve for c25s50 profile

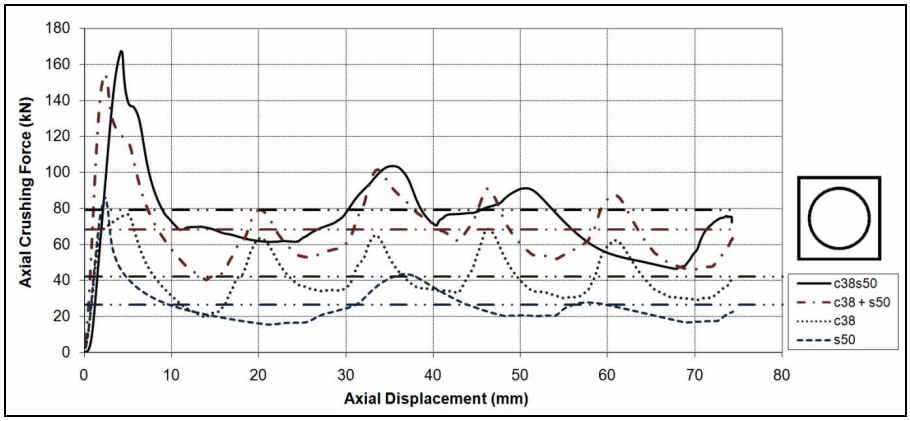

Figure 18: Force-displacement curve for c38s50 profile

with an increased wall thickness and same solidity ratio, using equations (2) and (3). The solidity ratio, introduced by Pugsley [27], is defined as the ratio of the cross-sectional area of the thin-wall structure to the cross-sectional area enclosed by the cross-section (equation (1)).

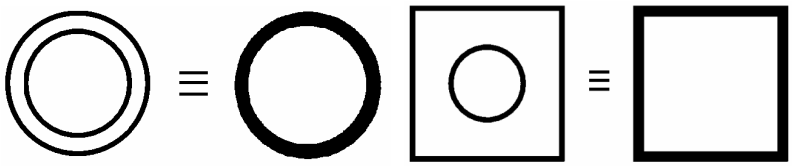

(a) (b)

Figure 19: Double cell profile with its equivalent single-cell (a) circular (b) square

Solidity ratio

$$\phi = A/A_c \tag{1}$$

For a thin-walled circular tube

$$\phi = 2H/R \tag{2}$$

And for thin-walled square tube

$$\phi = 4H/C \tag{3}$$

The theoretical quasi-static mean crushing force is calculated using equations (4) and (5), as defined by Jones [14]. For a circular tube, axi-symmetric axial crushing

$$P_m = \frac{2\left(\pi H\right)^{\frac{3}{2}} R^{\frac{1}{2}} \sigma_y}{3^{\frac{1}{4}} \left\{0.86 - 0.37\left(\frac{H}{R}\right)^{\frac{1}{2}}\right\}} \tag{4}$$

For a square tube, symmetric axial crushing

$$\frac{P_m}{M_o} = 52.22\sqrt[3]{\frac{C}{H}} \tag{5}$$

where $M_o = \frac{\sigma_y H^2}{4}$

The ultimate peak crushing force for a thin-walled circular tube was shown by Gupta and Gupta [9] to be given by

$$P_{ult} = \left(0.026 \times \frac{2R}{H} + 1.04\right) P_m \tag{6}$$

Following the same procedure used by Gupta and Gupta [9] and using the experimental data, the ultimate peak crush force for thin-walled square tubes is found to be related to the mean crushing force by

$$P_{ult} = \left(0.090 \times \frac{C}{H} + 0.446\right) P_m \tag{7}$$

In order to achieve good vehicle crashworthiness the common agreement among researchers [14,24] is to have an energy absorption device that achieves one or both of the following; decrease the initial peak force and/or absorb as much energy as possible. In fulfilling these criteria the device will enable a reduction in the acceleration perceived by vehicle occupants and the amount of energy transferred from the vehicle to its occupants in a crash. Crush force efficiency (CFE), given in equation (8) is a typical parameter used to assess the performance of energy absorbing devices in achieving these criteria.

$$CFE = \frac{P_m}{P_{ult}} \tag{8}$$

The ideal value for CFE is unity [7]. The CFE for the double-cell profile tubes is compared to that predicted for theoretical single-cell equivalent tubes. The CFE parameter is useful in determining the extent to which a constant deceleration is achieved, thus a value of unity would indicate that the device has reduced the ultimate peak force (P_{ult}) sufficiently to enable a smooth deceleration during impact. The results are listed in Table 4 and are graphically represented in Figure 20. The circular tubes are better as crash components compared to their square counterparts since they have higher CFE. For double-cell profiles with circular outer tubes there is a decrease in CFE when compared with their single-cell circular equivalent tubes. Similarly with the double-cell profiles with square outer tubes, the s25s50 and c38s50 profiles also have a decrease. The s25s50 profile shows a marked increase in CFE while the c25s50 has a slight increase.

The specific energies of the double-cell profiles are compared to the equivalent single-cell equivalent tube in Figure 21. The analysis suggests that single-cell circular equivalent tubes have a higher energy absorbing efficiency than their double-cell profiles it is the converse with

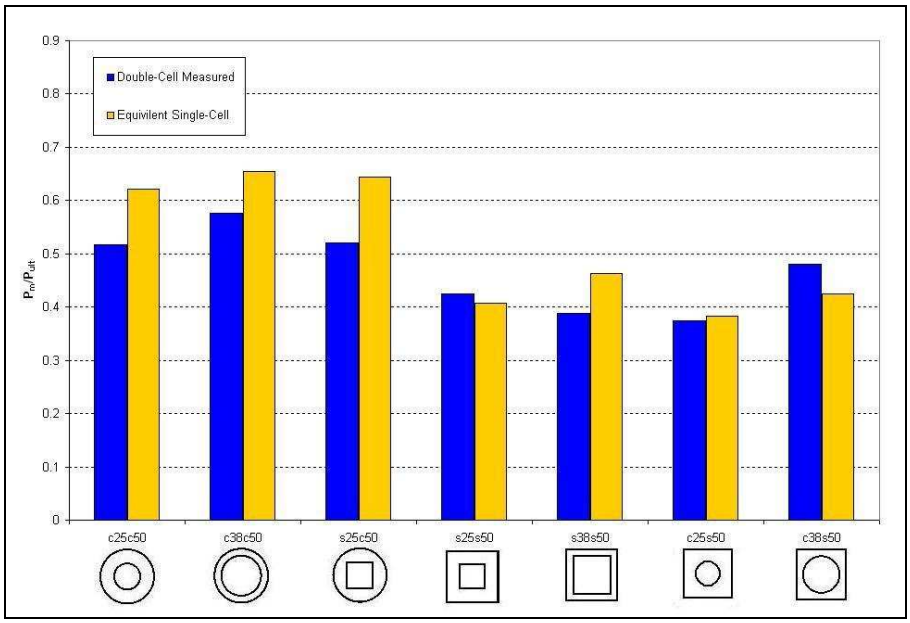

Figure 20: CFE for the different double-cell profiles compared with equivalent single cell profile

Table 4: Multi-cell profile tubes and their single-cell equivalent tubes and CFE

Multi-Cell Profile	**Solidity Ratio**	**Equivalent Tube (mm)**	**Equivalent Tube Wall Thickness (mm)**	**Double-Cell CFE**	**Equivalent Single-Cell CFE**
c25c50	0.18	ϕ50.8	2.24	0.52	0.62
c38c50	0.21	ϕ50.8	2.61	0.58	0.65
s25c50	0.20	ϕ50.8	2.48	0.52	0.64
s25s50	0.18	50.8 x 50.8	2.25	0.42	0.41
s38s50	0.21	50.8 x 50.8	2.64	0.39	0.46
c25s50	0.17	50.8 x 50.8	2.08	0.37	0.38
c38s50	0.19	50.8 x 50.8	2.36	0.48	0.42

single-cell square equivalent tubes. The double-cell profiles with square outer tubes have higher energy absorbing efficiencies than their single-cell square equivalent tubes. Circular tubes also have higher specific energies than their square counterparts.

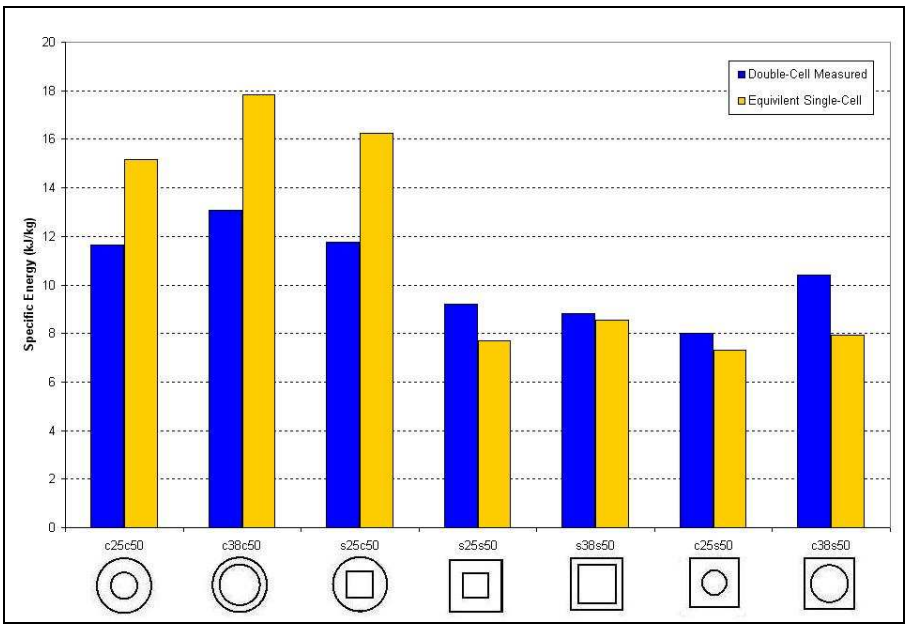

Figure 21: Specific energies of all double-cell profiles compared with equivalent single cell profile

2.4 Dynamic axial compression

The test rig used for the dynamic impact testing is a 7m high drop tester. The support arrangement (anvil) for the test specimens consists of two steel blocks of mass 430kg each on the laboratory floor. The test specimens are clamped at the lower end by means of a clamping rig, the same one used for the quasi-static tests, bolted to the top of one of the steel blocks. To ensure a central impact, the striker and the anvil is aligned in such a way that the centre of the striker matches the centre bore hole of the anvil. Prior to testing, the trolley is loaded with the required drop mass and raised to a 3m drop height (equivalent impact velocity of 7.67m/s assuming no energy losses). The trolley is released by a pneumatic piston and drops onto the free top edge of the tube under gravitational force.

Results from the dynamic axial loading tests are shown in Table 5 for the single-cell tubes and in Table 6 for double cell tubes. No transient experimental data measurement, such as displacement, velocity and acceleration history, is captured for the drop tests. A qualitative analysis of the results is performed, using drop height, impact energy and final crushed distance, and compared with the quasi-static test results. The single cell tubes buckle in the progressive

modes with lobe forming from the impacted end developing towards the non-impact end.

2.5 Single-cell tubes subjected to dynamic loading

Table 5: Dynamic crushing results for single cell tubes

Specimen	**h (m)**	**M (kg)**	V_i **(m/s)**	δ**(mm)**	E_{pd} **(kJ)**	P_m^d **(kN)**	**CM**
c38d1	3.00	202.9	7.68	74.2	6.13	82.5	Mixed
c38d3	3.00	202.9	7.68	58.2	6.09	104.7	Mixed
c38d4	2.00	169.4	6.26	51.7	3.41	65.9	Mixed
c50d1	3.00	202.9	7.67	69.3	6.11	94.9	Asymmetric
c50d2	3.00	266.5	7.67	99.9	8.11	87.3	Asymmetric
c50d3	3.00	169.4	7.67	54.5	5.08	100.3	Asymmetric
s38d1	2.25	202.9	6.64	99.1	4.67	47.1	Symmetric
s38d2	2.40	202.9	6.86	80.0	4.94	61.7	Symmetric
s38d3	2.00	202.9	6.26	71.4	4.12	57.8	Symmetric
s38d4	1.60	202.9	5.6	65.7	3.32	50.5	Symmetric
s50d1	1.29	202.9	5.03	60.8	2.69	44.3	Symmetric
s50d2	3.00	202.9	7.68	103.1	6.18	60.0	Symmetric
s50d5	3.00	169.4	7.67	83.0	5.12	61.7	Symmetric

2.6 Double-cell tubes subjected to dynamic loading

As observed for the quasi-static tests, the inner 25mm circular tube of the double cell profiles buckles in the Euler mode, as shown in Figure 22(a) and (b). The outer tube starts to buckle symmetrically in the progressive mode but changes buckling mode as a result of the interaction with the Euler deformation of the inner tube. In contrast, the inner 25mm square tube of the double cell tubes, shown in Figure 23, buckles either symmetrically or in mixed mode with little interaction with the outer tubes. Crushed distance increases with increasing drop heights, as expected because of the increase in drop energy.

For the c38c50 profile, both inner and outer tubes deformed in at axisymmetric mode, shown in Figure 24(a), with lobe forming from the impacted end. A transition from concertina to diamond buckling mode is observed for the inner tube when the drop mass is increased to 330kg (change in kinetic energy). Little interference is observed between the two circular tubes; the lobes of the inner tube just touch the lobes of the outer tube.

Figure 24(b) shows the crush shape of the c38s50 profile. The inner circular tube appears to start deforming in concertina mode at the impacted end. The outer square tube buckles symmetrically with lobe formation initiating at the non-impact end (except in the case when drop mass is 238.7kg). The lobes of the outer square tube then interfere with the inner circular

Table 6: Dynamic crushing results for double cell tubes

Specimen	**M (kg)**	δ**(mm)**	E_{pd}**(kJ)**	P_m^d **(kN)**	**Inner CM**	**Outer CM**
c25c50d1	202.9	45.9	6.06	132.1	Euler	Asymmetric
c25c50d2	266.5	60.1	8.01	133.2	Euler	Mixed
c25c50d3	327.8	87.4	9.92	113.6	Euler	Mixed
c38c50d1	202.9	29.9	6.02	201.7	Asymmetric	Asymmetric
c38c50d2	266.5	45.7	7.96	174.1	Asymmetric	Asymmetric
c38c50d3	329.8	61.9	9.91	160.2	Asymmetric	Asymmetric
c38c50d4	238.7	38.8	7.12	183.5	Asymmetric	Asymmetric
c38c50d5	361.5	69.8	10.88	156.0	Asymmetric	Asymmetric
s25c50d1	202.9	39.5	6.05	153.3	Symmetric	Asymmetric
s25c50d2	266.5	55.4	7.99	144.4	Euler	Asymmetric
s25c50d3	329.8	77.9	9.96	127.9	Euler	Asymmetric
s25c50d4	238.7	47.3	7.14	150.8	Euler	Asymmetric
s25c50d5	169.4	28.8	5.03	174.6	Symmetric	Asymmetric
s25s50d1	202.9	46.4	6.06	130.7	Symmetric	Symmetric
s25s50d2	266.5	59.7	8.00	134.0	Symmetric	Symmetric
s25s50d3	329.8	82.5	9.98	121.1	Symmetric	Symmetric
s25s50d4	238.7	54.9	7.16	130.4	Symmetric	Symmetric
s25s50d5	169.4	31.8	5.04	158.7	Symmetric	Symmetric
s38s50d1	202.9	42.4	6.28	148.1	Symmetric	Symmetric
s38s50d2	266.5	67.6	8.01	118.6	Symmetric	Symmetric
s38s50d3	266.5	62.0	8.01	129.3	Symmetric	Symmetric
s38s50d4	329.8	79.2	9.96	125.9	Symmetric	Symmetric
s38s50d5	238.7	53.6	7.15	133.4	Symmetric	Symmetric
s38s50d6	169.4	27.9	5.03	180.7	Symmetric	Symmetric
c25s50d1	202.9	66.1	6.11	92.4	Euler	Symmetric
c25s50d2	266.5	86.6	8.07	93.2	Euler	Symmetric
c38s50d1	202.9	41.9	6.06	144.7	Mixed	Symmetric
c38s50d2	266.5	56.6	7.99	141.2	Mixed	Symmetric
c38s50d3	329.8	89.9	10.00	111.2	Mixed	Symmetric
c38s50d4	238.7	48.7	7.14	146.7	Mixed	Symmetric
c38s50d5	169.4	29.8	5.03	169.2	Mixed	Symmetric

(a) (b)

Figure 22: Side and section view of dynamically crushed (a)c25c50 (b)c25s50

(a) (b)

Figure 23: Side and section view of dynamically crushed (a)c25s50 (b)s25s50

tube, forcing the inner tube to buckle at the same wavelength as the outer tube.

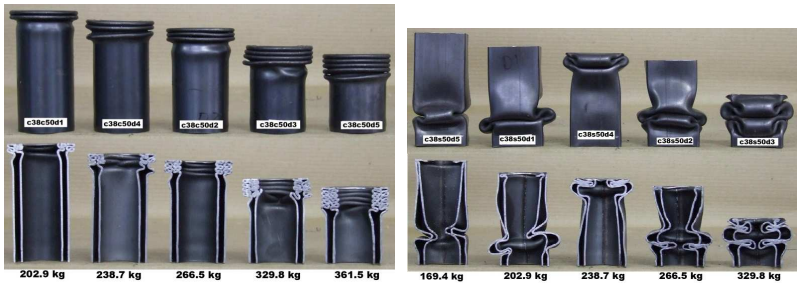

(a) (b)

Figure 24: Side and section view of dynamically crushed (a)c38c50 (b)c38s50

There is distinct interaction between the inner tube and outer tube of the s38s50 double-cell profile, shown in Figure 25. Both tubes deform symmetrically with lobes formed at similar wavelength. The lobe size of the inner tube is smaller than the lobe size of the outer tube.

Figure 25: Side and section view of dynamically crushed s38s50

Unlike the quasi-static tests, where an instantaneous axial crush force is recorded at an axial displacement, in dynamic axial crushing a pre-determined amount of energy results in a certain axial displacement. The specific energy for each double-cell tube is calculated for each drop test. The specific energy is then normalised with respect to the average yield strength of both tubes making the double-cell profile. Figure 26 shows the specific energy and crushed distance for each drop test and the data points are shown by a trend line. The legend on the right hand side of Figure 26 ranks the double-cell profile tubes in order of highest energy absorption efficiency. The c38c50 profile is the most efficient energy absorbing profile since for any axial displacement it has the highest specific energy. Similar to the quasi-static tests, the double-cell profiles with

circular outer tubes are more efficient than the double-cell profiles with square outer tubes. The c25s50 results are omitted in the graph because the c25 tube buckles in an Euler mode which is highly undesirable because of the lower energy absorption characteristic.

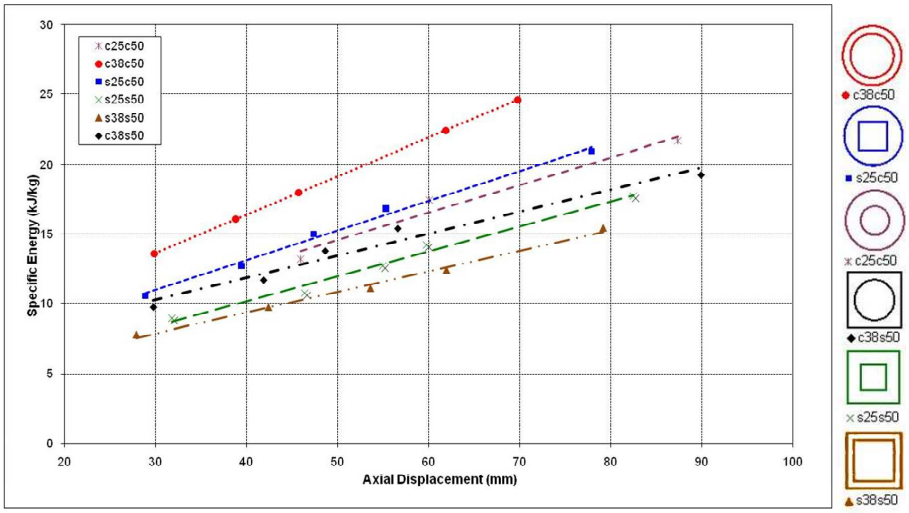

Figure 26: Specific energy versus axial displacement for the different double-cell profiles.

Figures 27 and 28 shows the specific energy, obtained from experiments, of the double cell profiles with circular outer tubes and square outer tubes respectively (dashed lines). These results are compared with the theoretical specific energy and predicted crushed distance of equivalent single cell profiles (solid lines) obtained using equation (9) for circular tubes and equation (10) for square tubes [14].

$$\delta = \frac{MV_i^2 \left\{ 2.14 \left(\frac{R}{H}\right)^{\frac{1}{2}} - 1 \right\}}{42.2\sigma_y RH \left\{ 1 + 0.41 \left(\frac{H}{R}\right)^{\frac{1}{2}} \right\} \left\{ 1 + \left(\frac{V_i}{4RD}\right)^{\frac{1}{\eta}} \right\}} \tag{9}$$

$$\delta = \frac{MV_i^2}{26.1\sigma_y H^2 \left(\frac{C}{H}\right)^{\frac{1}{3}} \left\{ 1 + \left(\frac{0.33V_i}{CD}\right)^{\frac{1}{\eta}} \right\}} \tag{10}$$

Figure 27 suggests that for shorter axial displacements the single-cell circular equivalent tubes are less efficient energy absorbers than the double-cell profiles with circular outer tube. The double cell profiles will have the same specific energy as the equivalent single cell profiles at the intersection of the solid and dashed lines. For the double cell profiles with c38 and s25 inner tubes the crushed distance would less than 40mm before the equivalent single cell become

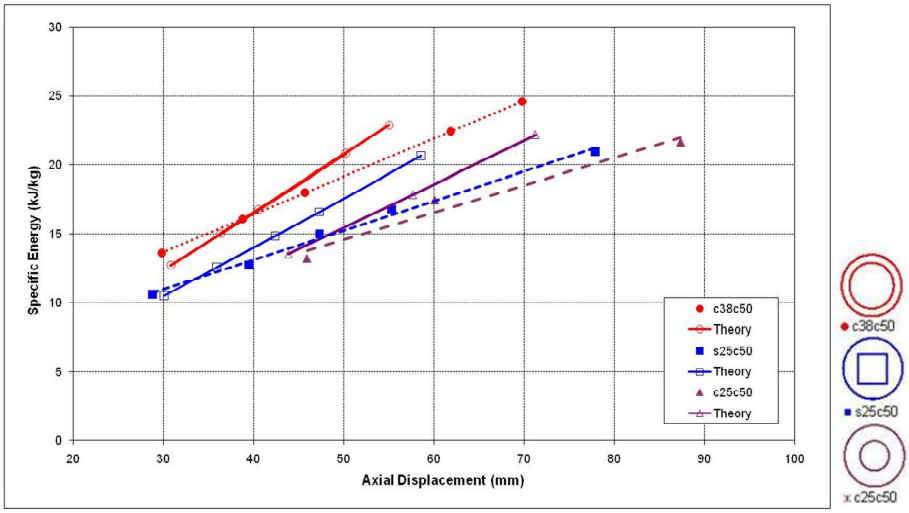

Figure 27: Specific energy for the double-cell profiles with a circular outer tube

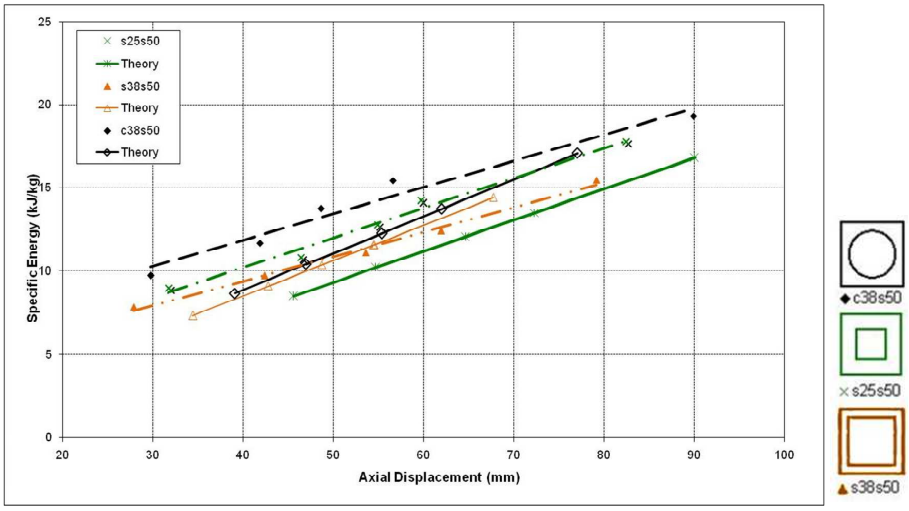

Figure 28: Specific energy for the double-cell profiles with a square outer tube

more efficient. For the double cell profile with the c25 inner tube it appears that the equivalent single cell profile is more efficient when the crushed distance is about 45mm.

Similar observations are made for the double cell profile with an outer square tube in Figure 28. Compared to the double cell profiles with circular outer tube, generally higher crushed distance is required before the equivalent single cell become more efficient that the double cell profiles with outer square tube. For double cell profiles with s38 inner tubes, the equivalent single cell becomes more efficient for crushed distances higher than 55mm. For double cell profiles with c38 inner tubes, a crushed distance of more than 85mm is required before the equivalent single cell profile becomes more efficient. However, in the case of the s25s50 double-cell profiles, the double cell profiles appear to be more energy efficient absorbers than the single cell equivalent.

3 Concluding remarks

Quasi-static and dynamic axial crush (impact masses ranging from 170-330kg with drop heights ranging from 1.3-3m) tests are performed on different mild steel single cell and double cells profiles. Initially, both tubes of a double cell profiles buckle independently with the outer tube dictating the lobe formation. Beyond a certain crushed distance, the inner tube appears to dominate the crushing mechanism as a result of the tubes interaction. Generally single circular tubes have better energy absorbing performance than single square tubes. This characteristic also applies for the double cell profile. In the case of double cell profiles with circular outer tubes, a theoretically equivalent single-cell circular tube is more efficient at absorbing energy than the double cell tube as equivalent single cell has higher CFE and specific energy. This would suggest that as crash components single cell tubes are better than the equivalent double cell profiles. However, while the results indicate that single cell tubes may absorb more energy, it has been observed experimentally that "thick" single cell tubes tend to tear when deformed plastically. In contrast a theoretically equivalent single-cell square tube is less efficient at absorbing energy than a double cell with square outer tube. There are numerous factors such as aspect ratios, imperfections and loading conditions that may cause tubes to buckle in Euler mode. For improved safety, the profiles that would buckle in Euler mode must be avoided as they are less efficient in absorbing energy.

4 Acknowledgements

The authors are indebted to the workshop staff, in particular Mr G. Newins, Mr L. Watkins and Mr. D. Jacobs of the Department of Mechanical Engineering of the University of Cape Town for manufacturing the test specimens.

References

[1] W. Abramowicz. Thin-walled structures as impact energy absorbers. Thin-Walled Structures, 41(2/3):91–107, 2003.

[2] A. Airoldi and G. Janszen. A design solution for a crashworthy landing gear with a new triggering mechanism for the plastic collapse of metallic tubes. Aerospace Science and Technology, 9:445–455, 2005.

[3] A.A.A. Alghamdi. Collapsible impact energy absorbers: an overview. Thin-Walled Structures, 39(2):189–213, 2001.

[4] B. Arnold and W. Altenhof. Experimental observations on the crush characteristics of aa6061 t4 and t6 structural square tubes with and without circular discontinuities. Int J Crash,, 9(1):73–87, 2004.

[5] R.S. Birch and N. Jones. Dynamic and static axial crushing of axially stiffened cylindrical shells. Thin walled Structures, 9(1/4):29–60, 1990.

[6] S.B. Bodlani, S. Chung Kim Yuen, and G.N. Nurick. The energy absorption characteristics of square mild steel tubes with multiple induced circular hole discontinuities. Part I: Experiments, J Appl Mech, In Press, 2009.

[7] Q. Cheng, W. Altenhof, and L. Li. Experimental investigations on the crush behaviouf of aa6061-t6 aluminium square tubes with different types of through-hole discontinuities. Thin-Walled Structures, 44(4):441–454, 2006.

[8] M. Elchalakani, X.L. Zhao, and R.H. Grzebieta. Tests on concrete filled double-skin (chs outer and shs inner) composite short columns under axial compression. Thin-Walled Structures, 40(5):415–441, 2002.

[9] N.K. Gupta and S.K. Gupta. Effect of annealing size and cutouts on axial collapse behaviour of circular tubes. Int J Mech Sci, 35(7):597–613, 1993.

[10] A.G. Hanssen, M. Langseth, and O.S. Hopperstad. Static crushing of square aluminium extrusions with aluminium foam filler. Int J Mech Sci, 41(8):967–993, 1999.

[11] A.G. Hanssen, M. Langseth, and O.S. Hopperstad. Axial crushing of aluminium columns with aluminium foam filler. 7th International Symposium on Structural Failure and Plasticity (IMPLAST 2000), pages 401–407, 2000.

[12] O.S. Hopperstad, M. Langseth, and A.G. Hanssen. Static and dynamic crushing of circular aluminium extrusions with aluminium foam filler. Int J Impact Eng, 24(5):475–507, 2000.

[13] O.S. Hopperstad, M. Langseth, and A.G. Hanssen. Optimum design for energy absorption of square aluminium columns with aluminium foam filler. Int J Mech Sci, 43(1):153–176, 2001.

[14] N. Jones. Structural impact. Cambridge University Press, 1989.

[15] N. Jones. Several phenomena in structural impact and structural crashworthiness. European Journal of Mechanics A/Solids, 22(5):693–707, 2003.

[16] N. Jones and R.S. Birch. Dynamic and static axial crushing of axially stiffened square tubes. Proceedings of the Institution of Mechanical Engineers, 204 (Part C):293–310, 1990.

[17] N. Jones and E.A. Papageorgiou. Dynamic axial plastic buckling of stringer stiffened cylindrical shells. Int J Mech Sci, 24(1):1–20, 1982.

[18] K. Kormi, D.C. Webb, C.N. Oguibe, and S.T.S. Al-Hassani. The dynamic and static axial crushing of axial stiffened square tubes–a comparison between numerical and experimental results. Crashworthiness and Occupant Protection in Transportation Systems, AMD-Vol. 210/BED-Vol. 30:143–160, 1995.

[19] B.E. Lampinen and R.A. Jeryan. Effectiveness of polyurethane foam in energy absorption structures. SAE Technical Paper Series, 820494, 1982.

[20] M. Langseth, T. Berstad, O.S. Hopperstad, and A.H. Clausen. Energy absorption in axially loaded square thin-walled aluminium extrusions. Structures Under Shock Impact III (SUSI III), pages 401–410, 1994.

[21] M. Langseth, A.G. Hanssen, and O.S. Hopperstad. Static and dynamic crushing of square aluminium extrusions with aluminium foam filler. Int J Impact Eng, 24(4):347–383, 2000.

[22] M. Langseth, O.S. Hopperstad, and A.G. Hanssen. Crash behaviour of thin-walled aluminium members. Thin-Walled Structures, 32(1/3):127–150, 1998.

[23] S. Lee, C. Hahn, M. Rhee, and J.E. Oh. Effect of triggering on the energy absorption capacity of axially compressed aluminium tubes. Materials and Design, 20(1):31–40, 1999.

[24] G. Lu and T. Yu. Energy Absorption of Structures and Materials. Woodhead Publishing Limited, 2003.

[25] R. Montanini, G. Belingardi, and R. Vadori. Dynamic axial crushing of tiggered aluminium thin-walled columns. 30th International Symposium on Automotive Technology and Automation, pages 437–444, 1997.

[26] G.N. Nurick and S. Chung Kim Yuen. The crushing charateristics of square tubes with blast-induced imperfections. Part II : Numerical Simulations, 2008.

[27] A.G. Pugsley and M. Macaulay. The large scale crumpling of thin cylindrical columns. Quarterly Journal of Mechanics and Applied Mathematics, 13(1):1–9, 1960.

[28] T.Y. Reddy and R.J. Wall. Axial compression of foam-filled thin-walled circular tubes. Int J Impact Eng, 7(2):151–166, 1988.

[29] S.R. Reid. Plastic deformation mechanisms in axial compressed metal tubes used as impact energy absorbers. Int J Mech Sci, 35(12):1035–1052, 1993.

[30] S.R. Reid, T.Y. Reddy, and M.D. Gray. Static and dynamic axial crushing of foam-filled sheet metal tubes. Int J Mech Sci, 28(5):295–322, 1986.

[31] S.P. Santosa, T. Wierzbicki, A.G. Hanssen, and M. Langseth. Experimental and numerical studies of foam-filled sections. Int J Impact Eng, 24(5):509–534, 2000.

[32] M. Seitzberger, F.G. Rammerstorfer, R. Gradinger, H.P. Degischer, M. Blaimschein, and C. Walch. Experimental studies on the quasi-static axial crushing of steel columns filled with aluminium foam. Int J Solids and Struc, 37(30):4125–4147, 2000.

[33] M. Seitzberger, R.F. Rammerstorfer, H.P. Degischer, and R. Gradinger. Crushing of axially compressed steel tubes filled with aluminium foam. Acta Mechanica, 125:93–105, 1997.

[34] G. Simic, V. Lucanin, and D. Milkovic. Elements of passive safety of railway vehicles in collision. Int J Crash,, 11(4):357–369, 2006.

[35] A.A. Singace. Collapse behaviour of plastic tubes filled with wood sawdust. Thin-Walled Structures, 37(2):163–187, 2000.

[36] J. Talonen and H. Hanninen. Effect of tensile properties on the energy-absorbing capacity of weld-bonded austenitic stainless steel profiles. Int J Crash, 11(4):371–378, 2006.

[37] P.H. Thornton. Energy absorption by foam filled structures. SAE paper 800081, 2005.

[38] P.H. Thornton and C.L. Magee. The interplay of geometric and materials variables in energy absorption. Transactions of the ASME–Journal of Engineering Materials and Technology, 99(2):114–120, 1977.

[39] A.K. Toksoy and M. Guden. The strengthening effect of polystyrene foam filling in aluminum thin-walled cylindrical tubes. Thin-Walled Structures, 43(3):333–350, 2005.

[40] M.D. White and N. Jones. Experimental quasi-static axial crushing of top-hat and double-hat thin walled sections. Int J Mech Sci, 41(2):179–208, 1999.

[41] M.D. White, N. Jones, and W. Abramowicz. A theoretical analysis for the quasi-static axial crushing of top-hat and double-hat thin walled sections. Int J Mech Sci, 41(2):209–233, 1999.

[42] S. Chung Kim Yuen, S.B. Bodlani, and G.N. Nurick. The energy absorption characteristics of square mild steel tubes with multiple induced circular hole discontinuities. Part II: Numerical Simulations, J Appl Mech, In Press, 2009.

[43] S. Chung Kim Yuen and G.N. Nurick. Modelling of axial loading of square tubes with blast-induced imperfections. Proceedings of 9th International Symposium on Plasticity and Impact Mechanics, IMPLAST 2007, pages 553–560, 2007.

[44] S. Chung Kim Yuen and G.N. Nurick. The crushing charateristics of square tubes with blast-induced imperfections. Part I : Experiments, J Appl Mech, In Press, 2008.

[45] S. Chung Kim Yuen and G.N. Nurick. The energy absorbing characteristics of tubular structures with geometric and material modifications: an overview. Applied Mechanics Reviews, 61(2):020802–1–020802–15, 2008.

[46] X.L. Zhao and R.H. Grzebieta. Strength and ductility of concrete filled double skin (shs inner and shs outer) tubes. Thin-Walled Structures, 40(2):199–213, 2002.

[47] X.L. Zhao, B. Han, and R.H. Grzebieta. Plastic mechanism analysis of concrete-filled double-skin (shs inner and shs outer) stub columns. Thin-Walled Structures, 40(10):815–833, 2002.